Surface & Coatings Technology 357 (2019) 78–82

Contents lists available at ScienceDirect

Surface & Coatings Technology

journal homepage: www.elsevier.com/locate/surfcoat

Corrosion protection and enhanced biocompatibility of biomedical Mg-Y-RE alloy coated with tin dioxide

Weihong Jin[a,b], Guomin Wang[b], Abdul Mateen Qasim[b], Shi Mo[b], Qingdong Ruan[b], Haili Zhou[a], Wei Li[a], Paul K. Chu[b,*]

[a] Institute of Advanced Wear & Corrosion Resistant and Functional Materials, Jinan University, Guangzhou 510632, China
[b] Department of Physics and Department of Materials Science and Engineering, City University of Hong Kong, Tat Chee Avenue, Kowloon, Hong Kong, China

ARTICLE INFO

Keywords:
Magnesium alloy
Corrosion
Biocompatibility
Surface modification
Tin dioxide

ABSTRACT

Oxide films composed of mainly tin dioxide and a small amount of stannous oxide are sputter-deposited onto the biomedical Mg-Y-RE (WE) alloy to enhance the anticorrosion properties and biocompatibility. The film composition, thickness, water contact angle, corrosion resistance, protein adsorption, and initial cell behavior are evaluated. Compared to the control, the corrosion current density and charge transfer resistance of the coated WE alloy in simulated body fluids show a 345-fold decrease and increase of more than 3 orders of magnitude, respectively, thus indicating excellent protection rendered by the surface layer. Furthermore, the modified WE alloy shows enhanced attachment and spreading of MC3T3-E1 pre-osteoblasts resulting from more protein adsorption.

1. Introduction

As a class of revolutionary orthopedic implant materials, magnesium (Mg) and its alloys have been extensively studied in recent years for potential application to fracture fixation devices and cardiovascular stents [1,2] due to natural degradation in the human body and elimination of potential follow-up surgeries after tissue healing [3]. However, rapid initial corrosion of Mg alloys in the aggressive physiological environment, which still remains the major challenge for clinical application [4], leads to excessive evolution of hydrogen bubbles, causes gas cavitation, and impedes initial cell attachment on the implant surface [5]. Mg dissolution also produces a local alkaline environment as well as excessive corrosion products causing adverse effects on cells [6,7]. Moreover, premature loss of mechanical integrity before tissue healing due to the unmatched corrosion rates can occur leading to failure of the implants before the expected end of service [3]. Consequently, fast initial degradation of Mg alloys must be controlled and the biocompatibility must also be enhanced in order that Mg alloys can be used more extensively as temporary implants.

Compared to the development of new types of Mg-based alloys, surface modification is a more economical and effective strategy to modulate the surface properties while preserving the intrinsic merits of the metallic implants by building a functional layer on Mg alloys [8–10]. Tin (Sn) is a trace and vital element and as an alloying element, Sn has recently been incorporated to develop novel biomedical Mg–1Sn and Mg–3Sn alloys with good mechanical properties, corrosion resistance, and cytocompatibility [11,12]. The excellent protection rendered by tin dioxide (SnO_2) was revealed by Wang et al. [13] who deposited fluorine-doped SnO_2 films on 317 L stainless steel by low-pressure chemical vapor deposition to retard corrosion of bipolar plates in polymer electrolyte membrane fuel cells. They observed a small and stable current from the SnO_2-deposited 317 L in the corrosive environment of 1 M H_2SO_4 + 2 ppm F^- solution at 70 °C. However, there have been limited studies on using Sn to modify biomedical Mg alloys. Ba et al. [14] reported that Sn ion implantation reduced dissolution of the GZ91K Mg alloy in simulated body fluids (SBF). The corrosion current density I_{corr} of the Sn-implanted alloy was reduced from 11.7 μA cm^{-2} of the untreated alloy to 5.74 μA cm^{-2} in SBF revealing less than one order of magnitude decrease. This transpires into limited improvement in the anticorrosion properties by Sn ion implantation and it may be due to metallic Sn in the modified layer as shown by the low binding energy of the Sn 3d XPS peak consequently accelerating galvanic corrosion. Meanwhile, application of a SnO_2 layer on Mg alloys to promote biological responses has not been reported so far. In this work, SnO_2 is deposited on the Mg-Y-RE (WE) alloy by reactive magnetron sputtering to enhance both the corrosion resistance and biocompatibility and the properties are assessed by electrochemical tests, contact angles, protein adsorption, and initial cell adhesion.

* Corresponding author.
E-mail address: paul.chu@cityu.edu.hk (P.K. Chu).

https://doi.org/10.1016/j.surfcoat.2018.10.005
Received 24 August 2018; Received in revised form 28 September 2018; Accepted 2 October 2018
Available online 03 October 2018
0257-8972/

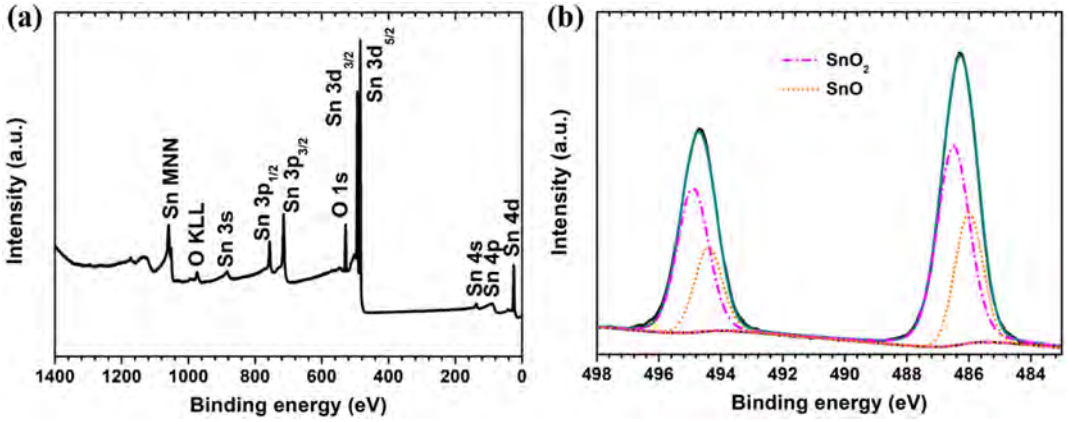

Fig. 1. (a) XPS full spectrum of SWE and (b) high-resolution spectrum with fitting of Sn 3d acquired from SWE after sputtering for 30 nm.

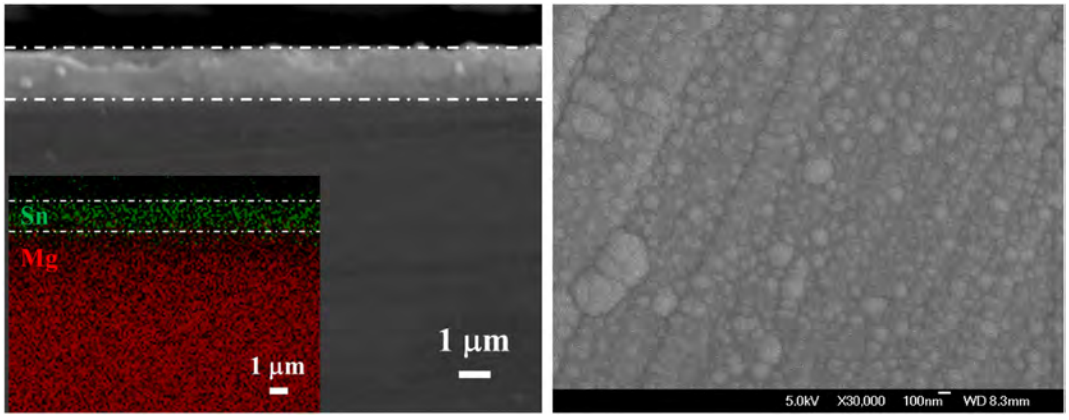

Fig. 2. (a) SEM and EDS analyses of the cross-sectional SWE and (b) Surface morphology of SWE observed by SEM.

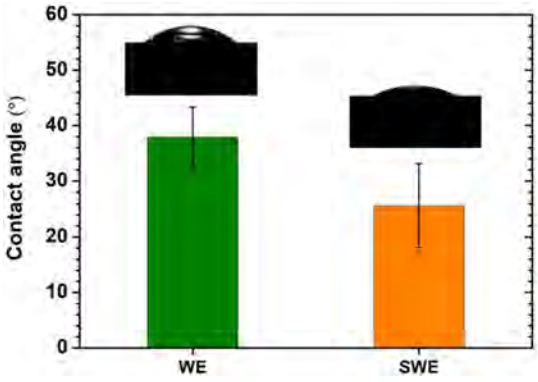

Fig. 3. Static water contact angles on the WE and SWE samples.

2. Experimental details

The WE Mg alloy plate was cut into 10 mm × 10 mm × 5 mm, ground with #2000 *SiC* abrasive paper, ultrasonically degreased in ethanol, and dried with nitrogen. The SnO_2 films were fabricated using a high purity Sn target in a reactive radio-frequency magnetron sputtering system (ATC-Orion 5 UHV, AJA International, Inc.) at a base pressure of 6.0×10^{-4} Pa. The flow rates of O_2 and Ar were 7 and 11 sccm during deposition, while the working pressure was 0.37 Pa. Deposition was conducted for 3 h at a power of 100 W without heating the substrate. The chemical composition of the fabricated films was determined by X-ray photoelectron spectroscopy (XPS) with a monochromatic Al K_α source (PHI 5802, Physical Electronics, Inc.) and the binding energies were calibrated to the C 1s line at 284.8 eV. The cross-section of the coated Mg alloy was analyzed by scanning electron microscopy (SEM, JSM-820, JEOL Ltd.) and the surface features of the deposited films on the WE alloy were examined by a field-emission SEM (JSM-6335F, JEOL Ltd.) equipped with energy-dispersive X-ray spectroscopy (EDS, INCAx-sight, Oxford Instruments). A contact angle goniometer (Model 200, Ramé-Hart) was employed in the static contact angle measurements at room temperature. A 4 μL droplet of distilled water was used and three measurements were carried out on different samples to obtain the average value.

To evaluate the corrosion behavior of the Mg alloy before and after modification, electrochemical impedance spectroscopy (EIS) and potentiodynamic polarization were carried out in simulated body fluid (SBF) at 37 °C on an electrochemical workstation (Zennium, Zahner). The electrochemical corrosion tests were conducted using a classical three-electrode cell system comprising a counter electrode (platinum sheet), reference electrode (saturated calomel electrode), and working electrode (sample). After immersion in SBF for 10 min, EIS was conducted from 100 kHz to 100 mHz with a 10 mV perturbing signal at the open circuit potential. Polarization tests were then conducted from −300 mV and 500 mV *versus* the open circuit potential at a scanning rate of 1 mV s^{-1} and I_{corr} and corrosion potential E_{corr} were derived by Tafel extrapolation according to a previous method [15].

Protein adsorption was assessed using Dulbecco's minimum essential medium (DMEM) supplemented with 10% Fetal Bovine Serum (FBS). The specimens were initially rinsed with phosphate-buffered saline (PBS) and soaked in 1 mL of DMEM + 10% FBS for 4 h at 37 °C. After incubation, the samples were washed with PBS and treated with 1% sodium dodecyl sulfate (SDS) under agitation for 1 h to desorb the proteins from the samples. The amount of proteins in the SDS solution was determined by the Micro-BCA Protein Assay Kit according to the

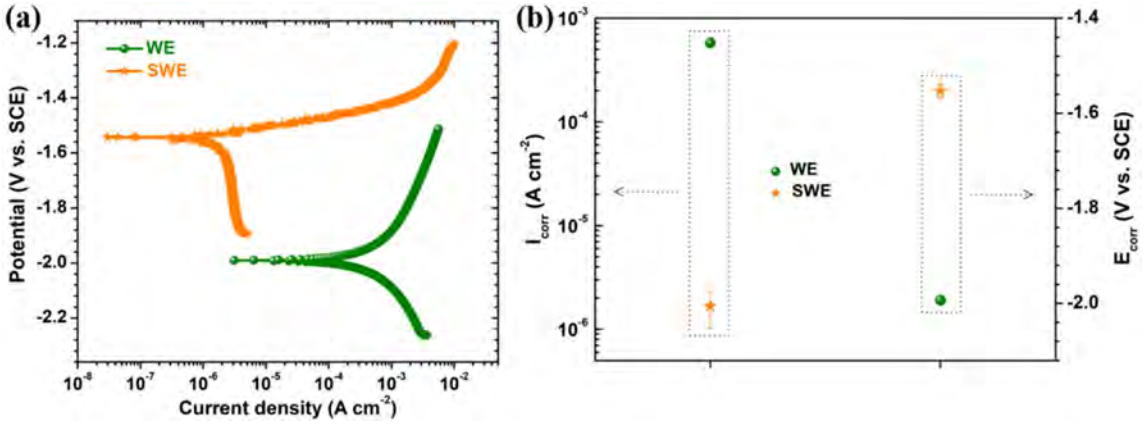

Fig. 4. (a) Polarization curves and (b) derived I_{corr} and E_{corr} of WE and SWE in SBF.

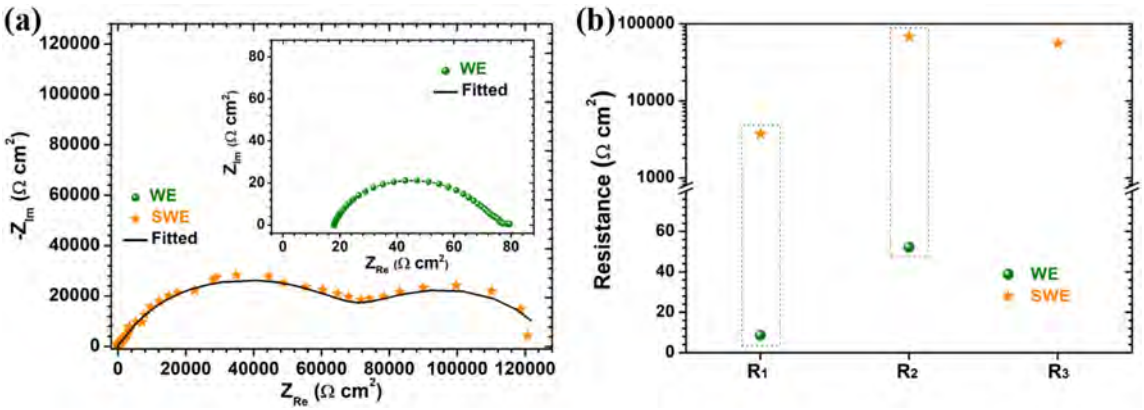

Fig. 5. (a) Nyquist plots and (b) calculated impedance of WE and SWE in SBF;

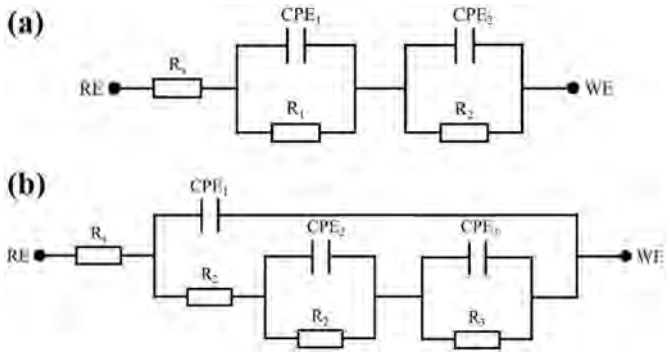

Fig. 6. Equivalent circuits used to fit the EIS data of (a) WE and (b) SWE in SBF.

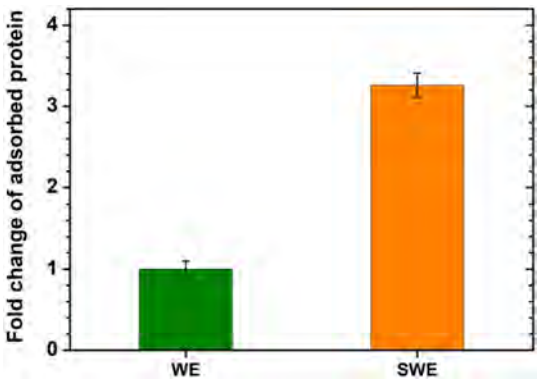

Fig. 7. Protein adsorption on the WE and SWE samples.

given protocol.

The MC3T3-E1 pre-osteoblasts cultured in DMEM supplemented with 10% FBS at 37 °C in a humidified atmosphere with 5% CO_2 were used to evaluate initial cell adhesion *in vitro*. 5×10^4 MC3T3-E1 cells were seeded on the sterilized samples on a 24-well culture plate. After incubation for 6 h, the seeded samples were rinsed with sterile PBS and fixed with 4% paraformaldehyde for 15 min. The cytoskeleton protein F-actin and nuclei were stained successively with fluorescein phalloidin and 4′,6-diamidino-2-phenylindole and the cell images were captured by a fluorescence microscope (Axio Observer Z1, Carl Zeiss).

3. Results and discussion

Fig. 1 presents the XPS full spectrum and high-resolution XPS spectrum of Sn 3d acquired from the modified WE Mg alloy after sputtering for 30 nm. According to the XPS full spectrum in Fig. 1a, only Sn and O are detected from the coated WE sample. As shown in Fig. 1b, the high-resolution XPS Sn 3d spectrum can be deconvoluted into the $3d_{5/2}$ and $3d_{3/2}$ doublets with a spin-orbital splitting of 8.4 eV and intensity ratio of 3:2. The high-resolution XPS spectra of Sn 3d show two peaks at 486.5 eV/494.9 eV and 486.0 eV/494.4 eV corresponding to SnO_2 and stannous oxide (SnO) [16,17], respectively. The atomic concentration ratio of SnO_2 reaches 66.6%. Thus, the WE alloy is covered by a surface layer mainly composed of SnO_2 with a minor amount of SnO. Fig. 2 shows the SEM cross-sectional view, corresponding elemental distributions, as well as surface morphology of the coated WE (SWE). As shown in Fig. 2a, the SWE sample has a sputtered surface layer with a thickness of 1.58 ± 0.08 μm. No obvious discontinuity is observed from the interface between the film and substrate. Fig. 2b shows that the surface of the modified Mg alloy is covered by a

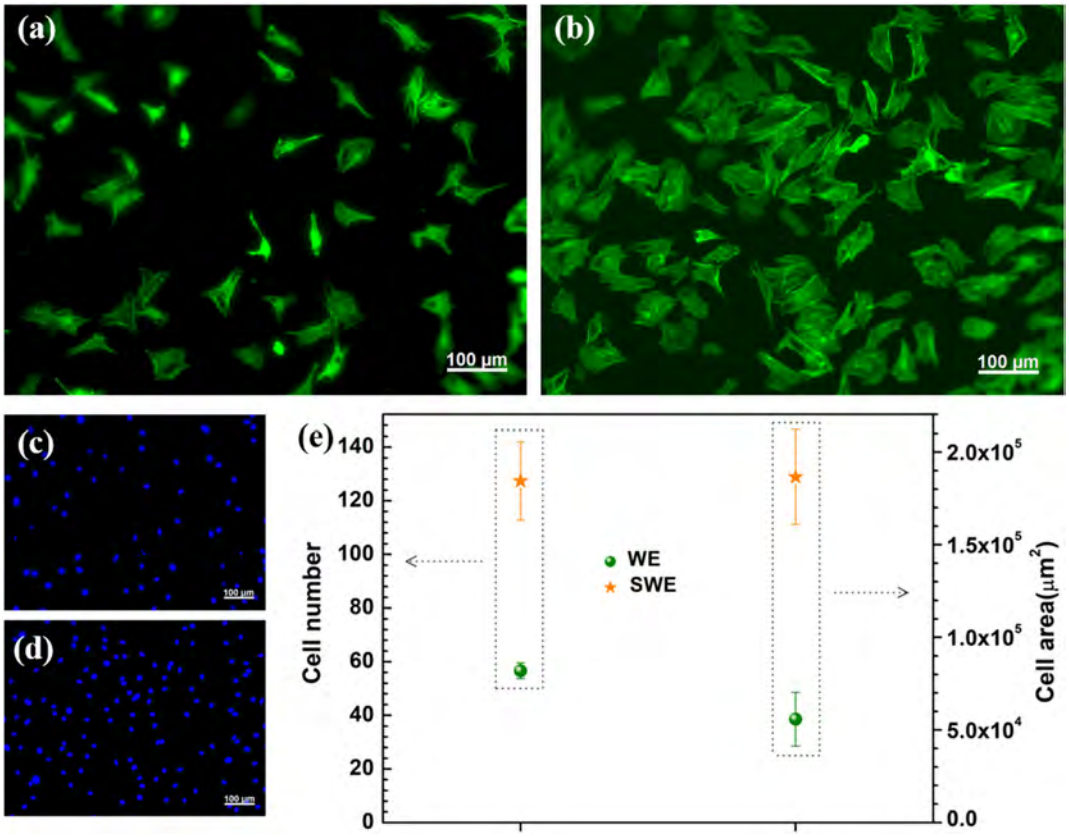

Fig. 8. Fluorescent images of the MC3T3-E1 pre-osteoblasts after incubation for 6 h on (a, c) WE and (b, d) SWE; (e) Cell number and area measured from (a, b) and (c, d), respectively.

continuous and dense film, although a few large particles are present on the film. The film on the WE substrate can act as a barrier to block penetration of species from the aggressive solution containing Cl^- to the Mg alloy thereby minimizing substrate destruction. Fig. 3 depicts the water contact angles of the WE and SWE samples. The water contact angle decreases from 37.9 ± 5.4° of the untreated WE sample to 25.7 ± 7.5°of the SWE sample. Since a smaller contact angle corresponds to higher hydrophilicity, the more hydrophilic SWE surface affects the surface interactions with proteins and cells.

Fig. 4a and b show the potentiodynamic polarization curves and I_{corr}, and E_{corr} of WE and SnO_2-deposited WE (SWE) in SBF. Compared to −1.993 ± 0.002 V of the bare WE, the corrosion potential of SWE in SBF rises to a more noble value of −1.553 ± 0.013 V, indicating a lower thermodynamic tendency towards electrochemical corrosion. The untreated WE control shows a corrosion current density of 580.4 ± 22.4 μA cm^{-2}, while that of the SWE Mg alloy decreases to 1.679 ± 0.656 μA cm^{-2}, corresponding to a 345-fold decrease. Wen et al. [18] observed a 59-fold decrease in I_{corr} from the HA/GO coated AZ31 alloy (36.43 ± 0.15 μA cm^{-2}) compared to the bare substrate (2124 ± 45 μA cm^{-2}) in SBF. Prakash et al. [19] observed a 4.2-fold decrease in I_{corr} from the nHAM-EDM treated Mg-Zn-Mn (22.7 μA cm^{-2}) compared to the bare substrate (5.43 μA cm^{-2}) in SBF. I_{corr} is a typical parameter to assess the kinetics of corrosion reactions and the efficiency of corrosion protection is generally proportional to I_{corr}. This remarkable reduction indicates that the corrosion resistance of the SWE sample is superior to the bare WE alloy. Consequently, dissolution of the WE substrate in SBF is mitigated by the protective SnO_2 film.

Fig. 5 shows the Nyquist plots and fitted impedances of the bare and modified WE alloys. Different equivalent circuits in Fig. 6 are used to fit the experimental data of WE and SWE since they have different time constants. The same equivalent circuit with three time constants in Fig. 6b has been reported for the PSPF-coated Mg–Gd–Y alloy [20] and PEO-coated Mg-Al_6-$Mn_{0.3}$-Sr_2 [21] immersed in the NaCl solution. As shown in Fig. 5a, the Nyquist plots of WE and SWE are fitted well with the corresponding equivalent circuits. R_s represents the electrolyte resistance, CPE_1 and R_1 are the capacitance and resistance of the film or corrosion products, respectively, CPE_2 and R_2 represent the double layer capacitance and charge transfer resistance, respectively, and CPE_3 and R_3 are the capacitance and resistance induced by the diffusion process in a finite region, respectively. The fitted impedances in Fig. 5b reveal that compared to the control, R_1 and R_2 of the SWE alloy are 3739 Ω cm^2 and 67,820 Ω cm^2 translating into 435-fold and 1300-fold increases, respectively. This implies that the SWE sample has a much higher film resistance and charge transfer resistance resulting in good film protection and mitigated dissolution of the Mg substrate. Bakhsheshi-Rad et al. [22] observed increased charge transfer resistance from 1680 Ω cm^2 of the bare Mg-1 wt%Ca-1 wt%Zn alloy to 3370 Ω cm^2 of the ZnO–coated sample and 7010 Ω cm^2 of the ZnO/$Ca_3ZrSi_2O_9$-coated sample in SBF, respectively. Kavitha et al. [23] observed increase in the film resistance and charge transfer resistance from 434 Ω cm^2 and 533 Ω cm^2 of the pure Mg to 14,230 Ω cm^2 and 8798 Ω cm^2 from the Sr-P coated Mg by HT at 200 °C in SBF, respectively. Our data provide evidence that the SnO_2 film provides better corrosion resistance on the WE Mg alloy in SBF. Regarding the SWE Mg alloy, transportation of the produced species is another factor inhibiting the corrosion process of the Mg substrate because R_3 reaches 55,610 Ω cm^2. Consequently, the EIS results suggest that corrosion of WE in SBF is remarkably mitigated by the oxide film and the results are consistent with the polarization tests. The stable SnO_2 plays the main role in retarding the dissolution of the WE substrate and the SnO reinforces the protection of the Mg alloy. The electrochemical study also reveals that the surface oxide layer even provides better protection than previously reported composite structures [18,19,22,23]. As a result,

SnO_2 can also be adopted as an intermediate layer in a composite structure to achieve better multifunctional properties.

From the perspective of biomedical implants, living tissues interact with the adsorbed protein layer on the implant surface instead of the original implant surface and the presence of adsorbed proteins on the surface of implant materials is essential in mediating cellular response to the implants [24]. Fig. 7 demonstrates that the SWE sample adsorbs more proteins than the bare WE sample after soaking in the cell culture medium possibly due to the increased surface hydrophilicity of the modified surface [25]. Higher protein adsorption further enhances the interaction between the materials surface and cells. To explore the status of initial cell attachment, MC3T3-E1 pre-osteoblasts are seeded on the bare and treated WE samples and observed by fluorescence microscopy. As shown in Fig. 8a–d, after incubation for 6 h, the pre-osteoblasts on the bare control are less in quantity, while more cells attach to the SWE surface. Furthermore, the pre-osteoblasts seeded on the WE surface show an abnormal shrunken morphology, whereas cells on the SWE sample spread much better with an elongated shape and more expression of filamentous actin. Fig. 8e shows that the average number and total surface area of attached cells on the WE sample are 57 and 55,818 μm^2, while those on the SWE sample reach to 127 and 186,520 μm^2, respectively. Therefore, the biological tests conducted *in vitro* suggest that the SnO_2 layer also improves initial cellular adhesion. The abundant absorbed proteins contribute to the higher degree of increased cell attachment and spreading on the SWE samples and are essential prerequisites for subsequent cell growth and proliferation [26].

4. Conclusion

The deposited film consisting of mainly SnO_2 and a small amount SnO offers good corrosion protection on the WE Mg alloy in the aggressive SBF as demonstrated by the smaller corrosion current density and higher impedance indicating that the modified surface layer is effective in mitigating surface corrosion. Pre-osteoblasts cultured on the modified WE alloy are larger in number and exhibit an elongated shape with more actin filaments thus indicating enhanced cell adhesion and spreading due to more proteins adsorption on the hydrophilic surface. Further studies are necessary to explore the detailed biological response of the SnO_2 layer and direct applicability to biomedical implants *in vivo*.

Acknowledgements

This work is financially supported by City University of Hong Kong Research Grants Council (RGC) General Research Funds (GRF) Nos. CityU 11205617 and 11301215.

References

[1] Y.F. Zheng, X.N. Gu, F. Witte, Biodegradable metals, Mater. Sci. Eng. R. Rep. 77 (2014) 1–34.
[2] Y. Chen, Z. Xu, C. Smith, J. Sankar, Recent advances on the development of magnesium alloys for biodegradable implants, Acta Biomater. 10 (2014) 4561–4573.
[3] M.P. Staiger, A.M. Pietak, J. Huadmai, G. Dias, Magnesium and its alloys as orthopedic biomaterials: a review, Biomaterials 27 (2006) 1728–1734.
[4] F. Witte, V. Kaese, H. Haferkamp, E. Switzer, A. Meyer-Lindenberg, C.J. Wirth, H. Windhagen, In vivo corrosion of four magnesium alloys and the associated bone response, Biomaterials 26 (2005) 3557–3563.
[5] G. Song, Control of biodegradation of biocompatable magnesium alloys, Corros. Sci. 49 (2007) 1696–1701.
[6] F. Seuss, S. Seuss, M.C. Turhan, B. Fabry, S. Virtanen, Corrosion of mg alloy AZ91D in the presence of living cells, J Biomed Mater Res B Appl Biomater 99B (2011) 276–281.
[7] Z. Zhai, X. Qu, H. Li, K. Yang, P. Wan, L. Tan, Z. Ouyang, X. Liu, B. Tian, F. Xiao, W. Wang, C. Jiang, T. Tang, Q. Fan, A. Qin, K. Dai, The effect of metallic magnesium degradation products on osteoclast-induced osteolysis and attenuation of NF-kappa B and NFATc1 signaling, Biomaterials 35 (2014) 6299–6310.
[8] X. Li, X. Liu, S. Wu, K.W.K. Yeung, Y. Zheng, P.K. Chu, Design of magnesium alloys with controllable degradation for biomedical implants: from bulk to surface, Acta Biomater. 45 (2016) 2–30.
[9] H. Hornberger, S. Virtanen, A.R. Boccaccini, Biomedical coatings on magnesium alloys - a review, Acta Biomater. 8 (2012) 2442–2455.
[10] G. Wu, J.M. Ibrahim, P.K. Chu, Surface design of biodegradable magnesium alloys - a review, Surf. Coat. Technol. 233 (2013) 2–12.
[11] C.Y. Zhao, F.S. Pan, S. Zhao, H.C. Pan, K. Song, A.T. Tang, Preparation and characterization of as-extruded Mg-Sn alloys for orthopedic applications, Mater. Des. 70 (2015) 60–67.
[12] H.-Y. Ha, J.-Y. Kang, J. Yang, C.D. Yim, B.S. You, Role of Sn in corrosion and passive behavior of extruded Mg-5 wt%Sn alloy, Corros. Sci. 102 (2016) 355–362.
[13] H. Wang, J.A. Turner, X. Li, R. Bhattacharya, SnO_2: F coated austenite stainless steels for PEM fuel cell bipolar plates, J. Power Sources 171 (2007) 567–574.
[14] Z. Ba, Q. Dong, J. Yin, J. Wang, B. Ma, X. Zhang, Z. Wang, Surface properties of Mg-Gd-Zn-Zr alloy modified by Sn ion implantation, Mater. Lett. 190 (2017) 90–94.
[15] W. Jin, G. Wu, H. Feng, W. Wang, X. Zhang, P.K. Chu, Improvement of corrosion resistance and biocompatibility of rare-earth WE43 magnesium alloy by neodymium self-ion implantation, Corros. Sci. 94 (2015) 142–155.
[16] J.F. Moulder, W.F. Stickle, P.E. Sobol, K.D. Bomben, Handbook of X-ray Photoelectron Spectroscopy, Perkin-Elmer Corporation, Eden Prairie, 1992.
[17] M. Kwoka, L. Ottaviano, M. Passacantando, S. Santucci, G. Czempik, J. Szuber, XPS study of the surface chemistry of L-CVD SnO_2 thin films after oxidation, Thin Solid Films 490 (2005) 36–42.
[18] C. Wen, X. Zhan, X. Huang, F. Xu, L. Luo, C. Xia, Characterization and corrosion properties of hydroxyapatite/graphene oxide bio-composite coating on magnesium alloy by one-step micro-arc oxidation method, Surf. Coat. Technol. 317 (2017) 125–133.
[19] C. Prakash, S. Singh, B.S. Pabla, M.S. Uddin, Synthesis, characterization, corrosion and bioactivity investigation of nano-HA coating deposited on biodegradable Mg-Zn-Mn alloy, Surf. Coat. Technol. 346 (2018) 9–18.
[20] X. Guo, K. Du, Q. Guo, Y. Wang, R. Wang, F. Wang, Effect of phytic acid on the corrosion inhibition of composite film coated on Mg–Gd–Y alloy, Corros. Sci. 76 (2013) 129–141.
[21] R.O. Hussein, P. Zhang, X. Nie, Y. Xia, D.O. Northwood, The effect of current mode and discharge type on the corrosion resistance of plasma electrolytic oxidation (PEO) coated magnesium alloy AJ62, Surf. Coat. Technol. 206 (2011) 1990–1997.
[22] H.R. Bakhsheshi-Rad, E. Hamzah, A.F. Ismail, M. Aziz, M. Kasiri-Asgarani, E. Akbari, S. Jabbarzare, A. Najafinezhad, Z. Hadisi, Synthesis of a novel nanostructured zinc oxide/baghdadite coating on Mg alloy for biomedical application: in-vitro degradation behavior and antibacterial activities, Ceram. Int. 43 (2017) 14842–14850.
[23] R.J. Kavitha, K. Ravichandran, T.S.N. Sankara Narayanan, Deposition of strontium phosphate coatings on magnesium by hydrothermal treatment: characteristics, corrosion resistance and bioactivity, J. Alloys Compd. 745 (2018) 725–743.
[24] M.S. Lord, M. Foss, F. Besenbacher, Influence of nanoscale surface topography on protein adsorption and cellular response, Nano Today 5 (2010) 66–78.
[25] P. Amaravathy, S. Sowndarya, S. Sathyanarayanan, N. Rajendran, Novel sol gel coating of Nb_2O_5 on magnesium alloy for biomedical applications, Surf. Coat. Technol. 244 (2014) 131–141.
[26] K. Anselme, Osteoblast adhesion on biomaterials, Biomaterials 21 (2000) 667–681.